Electronic Supplementary Material (ESI) for CrystEngComm.

Hydrogen bonding supports the coordination sphere in lanthanide complexes of 7-azaindole-*N*-oxide

Oskar G. Wood, Leanne Jones and Chris S. Hawes

Supporting Information

1. **Structure of $[Cu_2(OMe)_2L_2]$** **2**
2. **Experimental Section** **3**
3. **X-ray Powder Diffraction Patterns** **4**
4. **X-ray Crystallography Data Tables and additional figures** **7**
5. **Additional Electronic Spectroscopy Figures and Data** **12**
6. **Mass Spectrometry Figures** **14**
7. **References** **16**

1. Structure of $[Cu_2(OMe)_2L_2]$

Trace quantities of blue crystals of the title compound were sporadically observed in preparations of complex **1**, though we were unable reliably produce this material as a pure phase. The structure, whose diffraction data were solved and refined in the monoclinic space group $P2_1/c$, is closely related to complex **1**, and consists of two copper ions bridged by two μ_2 methoxide ions and each capped by a deprotonated, chelating **L** anion as shown in Figure S1. The inter-copper distance is 2.9924(7) Å, while the bridging methoxides bond symmetrically to the two copper ions with Cu-O distances in the range 1.901(3) – 1.955(3) Å. The coordination behaviour of the **L** anions is essentially equivalent to that seen in complex **1**.

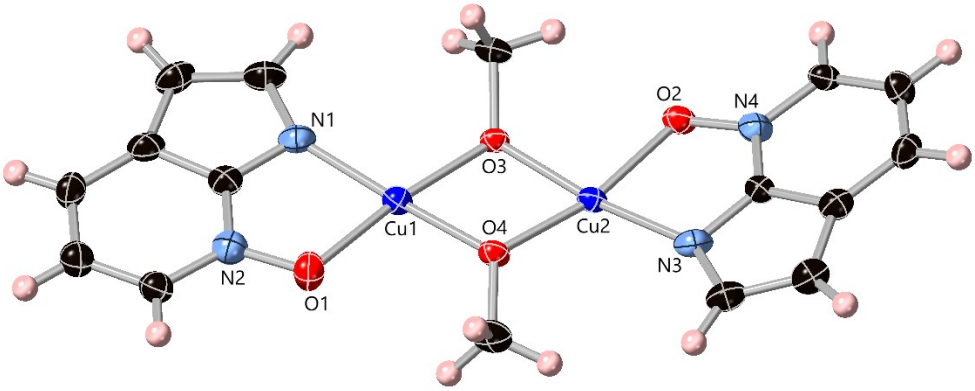

Figure S1 Structure of $[Cu_2(OMe)_2\mathbf{L}_2]$ with heteroatom labelling scheme. ADPs are rendered at the 50% probability level.

Furthermore, as with complex **1** adjacent complexes associate through long axial interactions between the copper centres and oxygen atoms from an adjacent complex. One of each of the methoxide and **L** anions engage in these interactions, with Cu-O distances 2.395(3) and 2.584(4) Å, respectively, such that four contacts exist between each pair of dimers as shown in Figure S2. The short distance between each dimeric unit causes the L units to buckle slightly outwards to achieve a more favourable separation for π···π interactions at the periphery, though the interatomic distance near the coordination sites (N1···N4) of 3.189(6) Å is still shorter than the ideal distance for an attractive interaction. These aggregates further associate through typical edge-to-face type interactions throughout the extended structure.

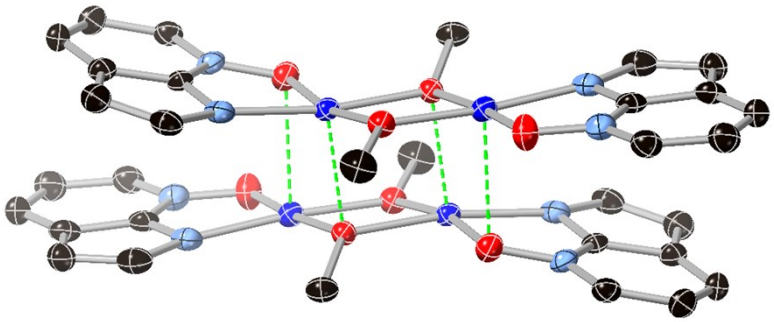

Figure S2 The dimeric assembly of adjacent complexes in the structure of $[Cu_2(OMe)_2\mathbf{L}_2]$ with weak axial interactions shown as green dashed lines. Hydrogen atoms are omitted for clarity.

2. Experimental Section

Materials and Methods

All reagents and solvents were purchased from Merck, Fluorochem or Alfa Aesar, and were used as received. Single crystals of **HL**·0.75H_2O were prepared by dissolution of 20 mg of commercial **HL** (Fluorochem) in 10 mL of acetonitrile, and allowing the solution to evaporate under air over the course of two weeks. When crystallising complexes **2** – **5** by antisolvent vapour diffusion, we observed the best reproducibility when the inner vessel (40 × 8.2mm straight-walled shell vial) was allowed to rest at an angle (*ca.* 30°) within the antisolvent chamber and not stood directly upright. High resolution mass spectra were collected in positive ion mode using an Agilent 6530 LC-QToF coupled to an Infinity II UPLC. HRMS samples were prepared by re-dissolving the crystalline products in either methanol or acetonitrile. Infrared spectra were recorded on a Thermo Nicolet iS10 spectrometer operating in ATR sampling mode. Melting points were recorded on an Electrothermal IA9000 instrument in air and are uncorrected. Elemental analyses were recorded using a Thermo Flash 2000 CHNS combustion analyser under He carrier gas, using vanadium pentoxide as a combustion aid and sulfanilamide standards. X-ray powder diffraction patterns were recorded at room temperature using a Bruker D8 Quest powder diffractometer with Cu Kα radiation (λ = 1.5406 Å) in the 2θ range 5 - 55°, with samples mounted on zero-background silicon plates. Electronic spectroscopy was performed using a Varian Cary 50 Bio Spectrophotometer and Varian Eclipse Fluorimeter, using quartz cuvettes of 1 cm path length (Starna) and spectrophotometric grade solvents (Alfa Aesar). Titrations in absorbance and emission were fitted to a 1M:3L equilibrium binding model using the non-linear least squares routine with ReactLab Equilibrium.[S1] All data in the range 550 – 725 nm were fitted for the phosphorescence spectra, while absorbance data were fitted in the range 340 – 250 nm to avoid interference from the free metal salt absorbance at higher energies. The presented stability constant is averaged from fits of 4 independent datasets.

X-ray Crystallography

Crystal and refinement data are presented as supporting information, Tables S1 and S2 (ESI). The diffraction data for all compounds were collected using a Bruker D8 Quest ECO single crystal diffractometer using graphite-monochromated Mo Kα radiation (λ = 0.7107 Å) and a Photon II C14 pixel array detector. The sample temperatures were maintained at 150 K throughout the collections using an Oxford Cryostream 800. Instrument control and data reduction were performed using the Bruker APEX-3 suite of programmes,[S2] and multi-scan absorption corrections were applied using SADABS.[S3] The diffraction data were solved with the intrinsic phasing routine in SHELXT,[S4] and refined on F^2 using least squares procedures in SHELXL,[S5] within the OLEX-2 GUI.[S6] All non-hydrogen atoms were refined anisotropically. Carbon-bound hydrogen atoms were refined with riding models, while (where data quality allowed) hydrogen atoms involved in hydrogen bonding were assigned on the basis of Fourier residuals and subsequently restrained with distance restraints and applied riding U_{iso} dependencies 1.5 times the isotropic equivalent of their carrier atoms. Where disorder was evident on the main residue in complex **3**, the two fragments were modelled separately with freely refined occupancy factors which were subsequently fixed to the nearest integer fraction, and internal DFIX and RIGU restraints were used to maintain sensible geometries for the two fragments.

3. X-ray Powder Diffraction Patterns

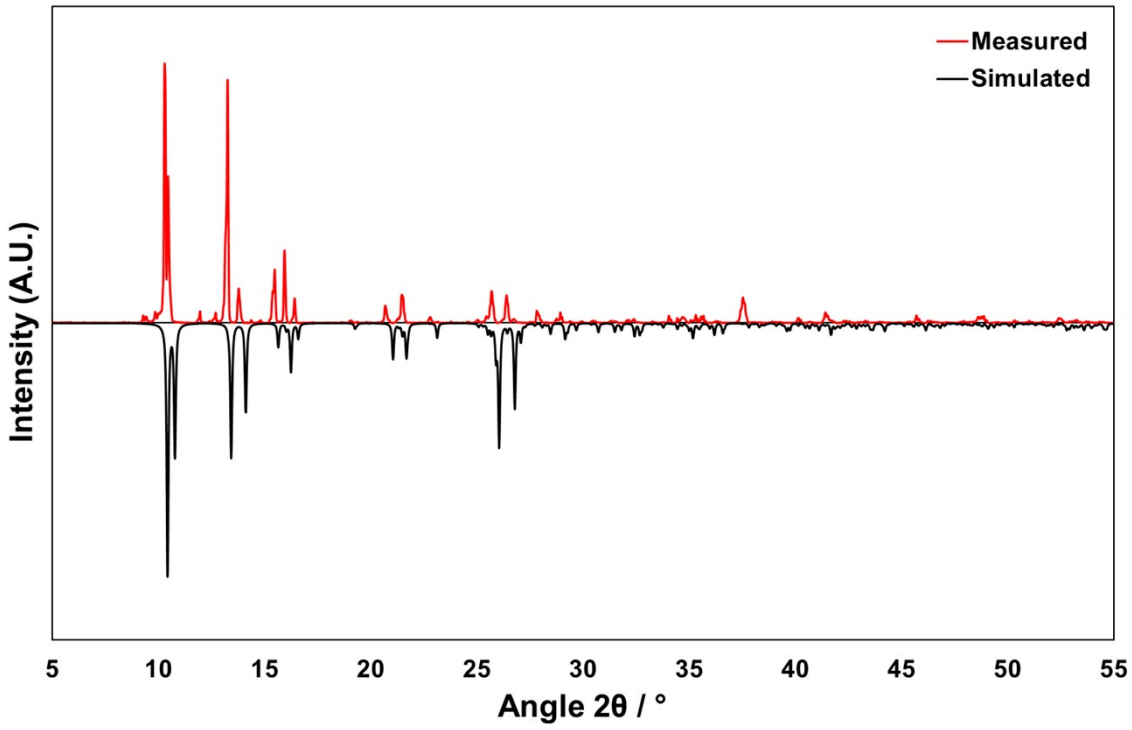

Figure S3 X-ray powder diffraction pattern for complex **1** (Red, room temperature) compared with simulated pattern (black, 150 K).

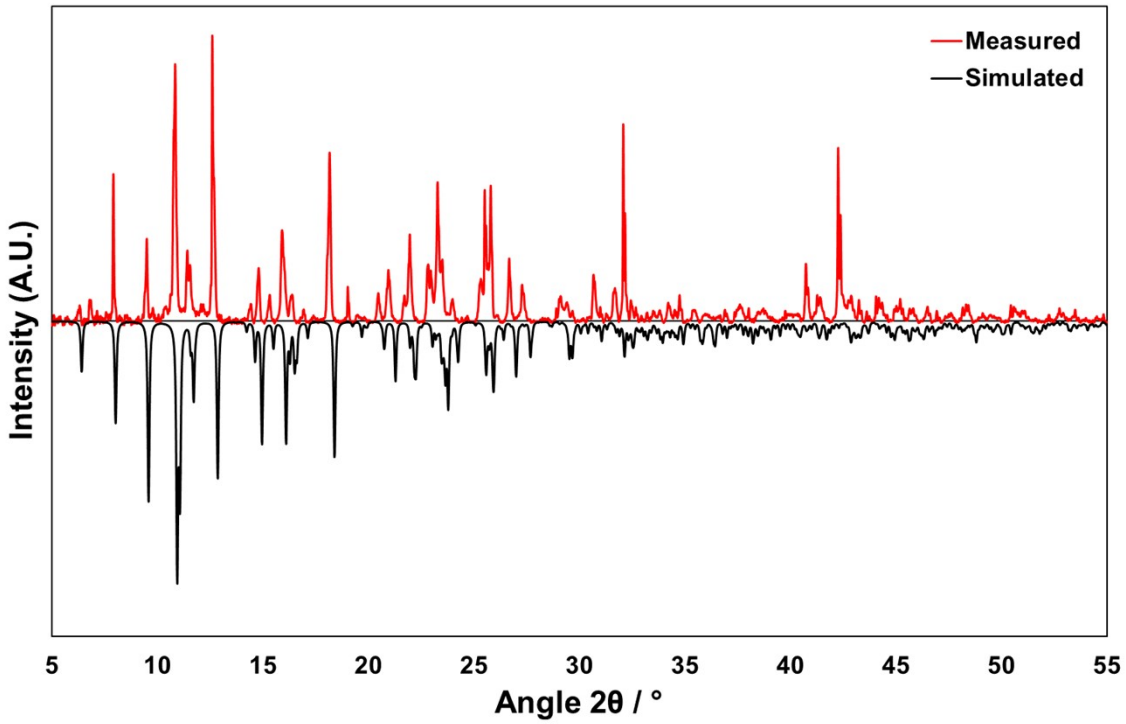

Figure S4 X-ray powder diffraction pattern for complex **2** (Red, room temperature) compared with simulated pattern (black, 150 K).

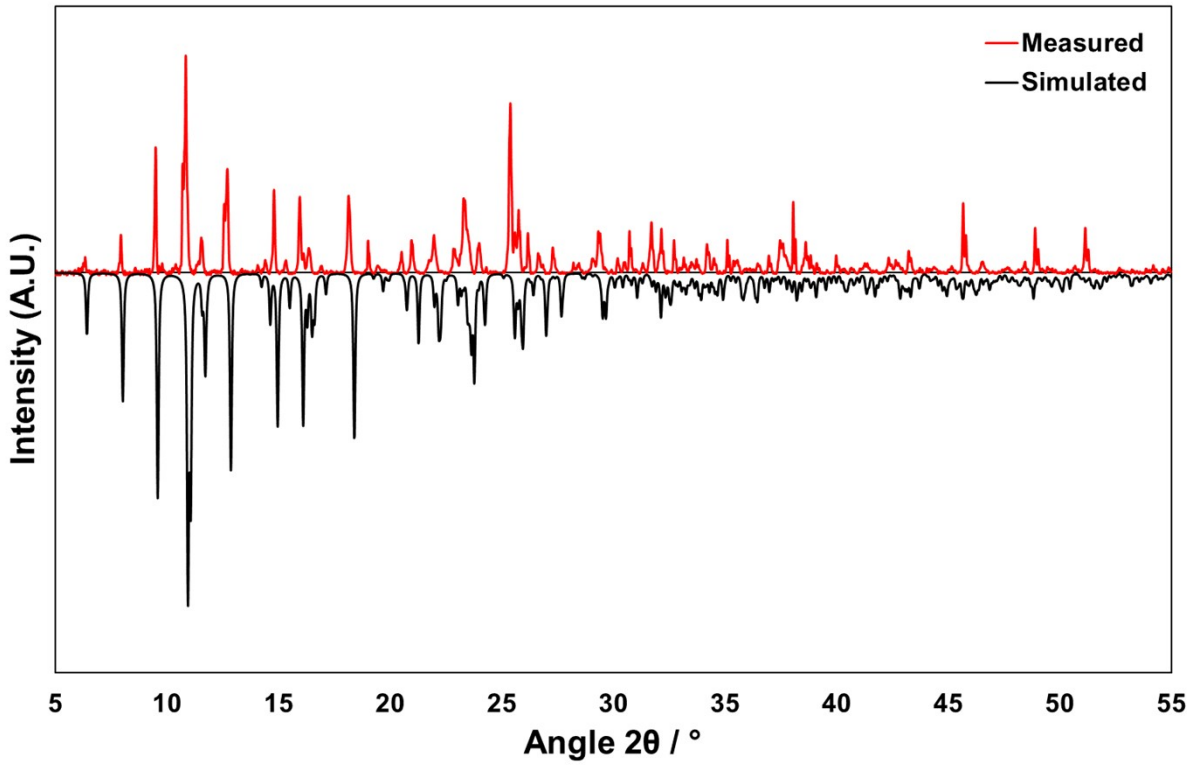

Figure S5 X-ray powder diffraction pattern for complex **3** (Red, room temperature) compared with simulated pattern (black, 150 K).

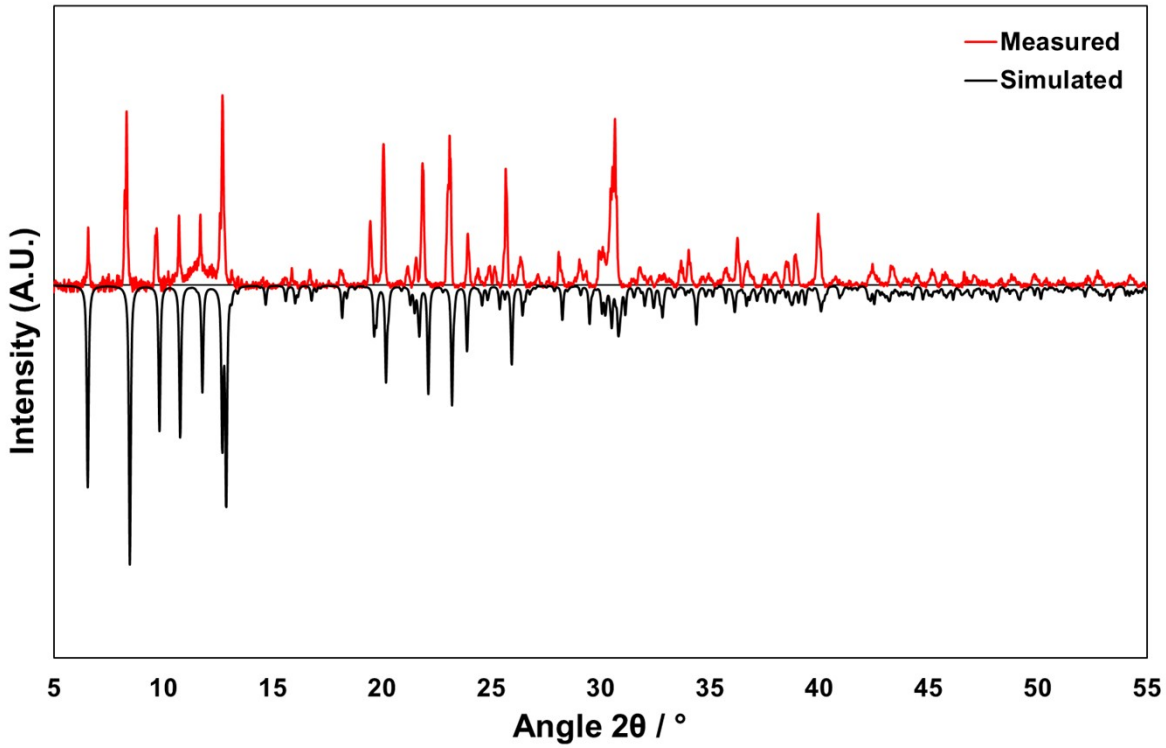

Figure S6 X-ray powder diffraction pattern for complex **4** (Red, room temperature) compared with simulated pattern (black, 150 K).

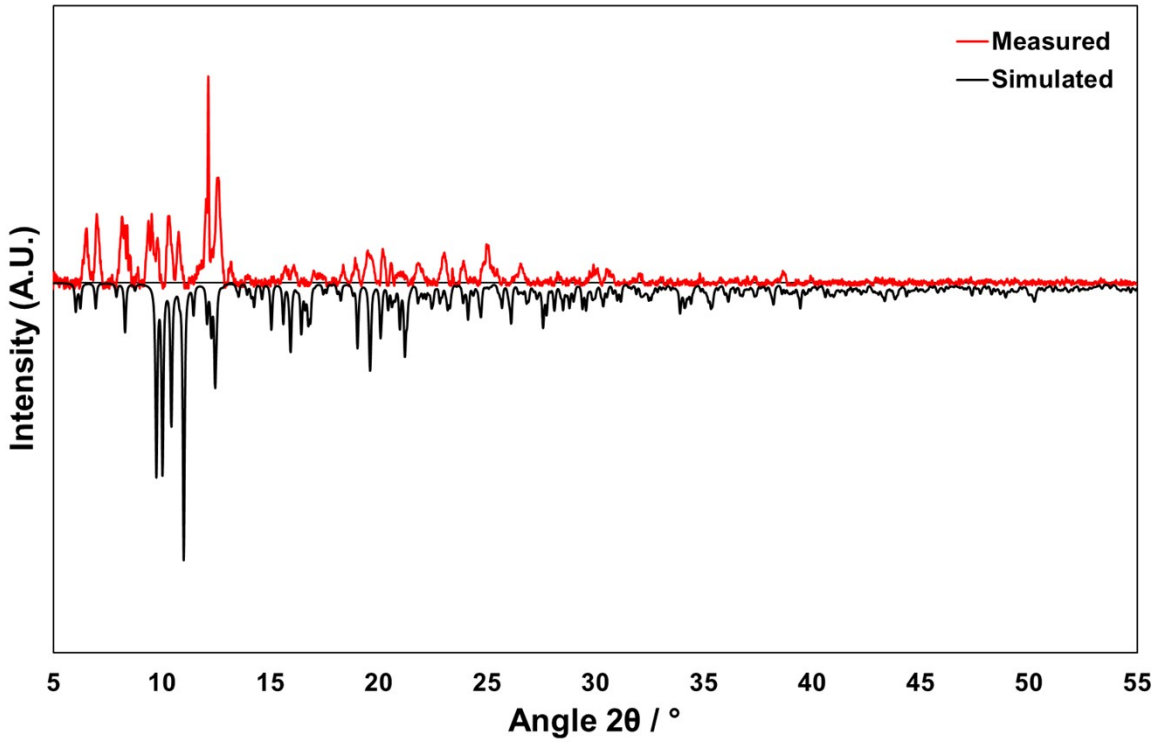

Figure S7 X-ray powder diffraction pattern for complex **5** (Red, room temperature) compared with simulated pattern (black, 150 K).

4. X-ray Crystallography Data Tables

Table S1 Crystal and Refinement Data for **L·0.75H_2O, 1** and **2**

Identification code	**L_0.75H_2O**	**1**	**2**
Empirical formula	$C_{28}H_{30}N_8O_7$	$C_{14}H_{10}CuN_4O_2$	$C_{21}H_{18}EuN_9O_{12}$
Formula weight	590.6	329.8	740.4
Temperature/K	150	150	150
Crystal system	monoclinic	monoclinic	triclinic
Space group	$P2_1/n$	$P2_1/n$	P-1
a/Å	19.0792(8)	8.6982(5)	8.5699(4)
b/Å	7.8359(4)	11.0452(6)	11.7452(6)
c/Å	19.1930(9)	13.7542(8)	14.2218(7)
α/°	90	90	78.6540(10)
β/°	94.0760(10)	106.867(2)	77.1540(10)
γ/°	90	90	70.8060(10)
Volume/Å^3	2862.1(2)	1264.57(12)	1306.15(11)
Z	4	4	2
ρ_{calc}g/cm^3	1.371	1.732	1.883
μ/mm^{-1}	0.101	1.737	2.484
F(000)	1240	668	732
Crystal size/mm^3	0.4 × 0.24 × 0.12	0.18 × 0.04 × 0.02	0.3 × 0.23 × 0.18
Radiation	MoKα (λ = 0.71073)	MoKα (λ = 0.71073)	MoKα (λ = 0.71073)
2Θ range for data collection/°	5.618 to 61.122	6.128 to 55.068	6.328 to 61.086
Index ranges	-27 ≤ h ≤ 27, -11 ≤ k ≤ 11, -27 ≤ l ≤ 25	-11 ≤ h ≤ 9, -14 ≤ k ≤ 14, -17 ≤ l ≤ 17	-12 ≤ h ≤ 12, -16 ≤ k ≤ 16, -20 ≤ l ≤ 20
Reflections collected	59294	15000	37986
Independent reflections	8783 [R_{int} = 0.0618, R_{sigma} = 0.0396]	2911 [R_{int} = 0.0569, R_{sigma} = 0.0495]	7957 [R_{int} = 0.0217, R_{sigma} = 0.0168]
Data/restraints/parameters	8783/10/418	2911/0/190	7957/3/397
Goodness-of-fit on F^2	1.042	1.029	1.169
Final R indexes [I>=2σ (I)]	R_1 = 0.0501, wR_2 = 0.1005	R_1 = 0.0403, wR_2 = 0.0788	R_1 = 0.0159, wR_2 = 0.0378
Final R indexes [all data]	R_1 = 0.0821, wR_2 = 0.1131	R_1 = 0.0684, wR_2 = 0.0892	R_1 = 0.0169, wR_2 = 0.0381
Largest diff. peak/hole / e Å^{-3}	0.28/-0.26	0.57/-0.40	0.49/-0.73
CCDC No.	2288060	2288061	2288062

Table S2 Crystal and Refinement Data for **3, 4** and **5**

Identification code	**3**	**4**	**5**
Empirical formula	$C_{21}H_{18}GdN_9O_{12}$	$C_{42}H_{36}Cl_6Eu_2N_{12}O_6$	$C_{56}H_{50}Cl_6N_{16}O_9Yb_2$
Formula weight	745.69	1321.45	1649.9
Temperature/K	150	150	150
Crystal system	triclinic	triclinic	triclinic
Space group	*P*-1	*P*-1	*P*-1
a/Å	8.5744(3)	8.4097(3)	13.2616(4)
b/Å	11.7399(4)	10.7232(4)	16.7698(6)
c/Å	14.2153(5)	13.8568(5)	16.9393(6)
α/°	78.6810(10)	79.1160(10)	118.4950(10)
β/°	77.1570(10)	80.1310(10)	93.0430(10)
γ/°	70.8240(10)	79.9150(10)	103.0590(10)
Volume/Å^3	1305.88(8)	1195.72(8)	3167.75(19)
Z	2	1	2
ρ_{calc}g/cm^3	1.896	1.835	1.73
μ/mm^{-1}	2.622	2.994	3.255
F(000)	734	648	1624
Crystal size/mm^3	0.25 × 0.21 × 0.2	0.16 × 0.1 × 0.08	0.17 × 0.09 × 0.04
Radiation	MoKα (λ = 0.71073)	MoKα (λ = 0.71073)	MoKα (λ = 0.71073)
2Θ range for data collection/°	6.326 to 57.41	5.322 to 56.67	4.892 to 52.878
Index ranges	-11 ≤ h ≤ 11, -15 ≤ k ≤ 15, -17 ≤ l ≤ 19	-11 ≤ h ≤ 11, -14 ≤ k ≤ 14, -18 ≤ l ≤ 18	-16 ≤ h ≤ 16, -20 ≤ k ≤ 20, -21 ≤ l ≤ 21
Reflections collected	27414	26086	62610
Independent reflections	6724 [R_{int} = 0.0228, R_{sigma} = 0.0200]	5964 [R_{int} = 0.0410, R_{sigma} = 0.0379]	12991 [R_{int} = 0.0793, R_{sigma} = 0.0702]
Data/restraints/parameters	6724/3/397	5964/174/394	12991/77/827
Goodness-of-fit on F^2	1.114	1.078	1.036
Final R indexes [I>=2σ (I)]	R_1 = 0.0174, wR_2 = 0.0379	R_1 = 0.0331, wR_2 = 0.0603	R_1 = 0.0446, wR_2 = 0.0743
Final R indexes [all data]	R_1 = 0.0192, wR_2 = 0.0384	R_1 = 0.0454, wR_2 = 0.0644	R_1 = 0.0832, wR_2 = 0.0852
Largest diff. peak/hole / e Å^{-3}	0.45/-0.70	2.12/-1.36	1.14/-0.86
CCDC No.	2288063	2288064	2288065

Table S3 Crystal and Refinement Data for $[Cu_2L_2OMe_2]$

Identification code	**$Cu_2L_2OMe_2$**
Empirical formula	$C_{16}H_{16}Cu_2N_4O_4$
Formula weight	455.41
Temperature/K	150
Crystal system	Monoclinic
Space group	$P2_1/c$
a/Å	12.4309(6)
b/Å	10.4129(5)
c/Å	13.1342(6)
α/°	90
β/°	104.761(2)
γ/°	90
Volume/Å^3	1644.00(14)
Z	4
ρ_{calc}g/cm^3	1.84
μ/mm^{-1}	2.619
F(000)	920
Crystal size/mm^3	0.06 × 0.05 × 0.02
Radiation	MoKα (λ = 0.71073)
2Θ range for data collection/°	5.616 to 56.57
Index ranges	$-16 \le h \le 16$, $-13 \le k \le 13$, $-15 \le l \le 17$
Reflections collected	33543
Independent reflections	4084 [R_{int} = 0.1167, R_{sigma} = 0.0742]
Data/restraints/parameters	4084/0/237
Goodness-of-fit on F^2	1.102
Final R indexes [I>=2σ (I)]	R_1 = 0.0632, wR_2 = 0.0991
Final R indexes [all data]	R_1 = 0.1063, wR_2 = 0.1104
Largest diff. peak/hole / e Å^{-3}	0.82/-0.59
CCDC No.	2288066

Table S4 Hydrogen bonding parameters for L·0.75H_2O

D	H	A	d(D-H)/Å	d(H-A)/Å	d(D-A)/Å	D-H-A/°
N1	H1	O2[1]	0.906(14)	1.803(14)	2.7018(15)	171.7(16)
N3	H3	O1[2]	0.882(13)	1.874(14)	2.7518(15)	173.4(16)
N5	H5A	O4	0.886(14)	1.890(14)	2.7714(16)	173.6(17)
N7	H7A	O3	0.898(14)	1.853(14)	2.7457(15)	172.4(16)
O5	H5B	O6	0.887(15)	1.773(16)	2.6510(16)	170(2)
O5	H5C	O2	0.877(16)	1.840(16)	2.7147(15)	175(2)
O6	H6A	O5[3]	0.873(15)	1.805(16)	2.6750(17)	174(2)
O6	H6B	O3	0.874(15)	1.821(16)	2.6843(16)	169(2)
O7	H7B	O4	0.871(15)	1.934(15)	2.8044(14)	178(2)
O7	H7C	O1[4]	0.872(15)	1.942(15)	2.8145(14)	180(2)

[1]+*x*,-1+*y*,+*z*; [2]+*x*,1+*y*,+*z*; [3]3/2-*x*,-1/2+*y*,1/2-*z*; [4]1/2+*x*,1/2-*y*,1/2+*z*

Table S5 Hydrogen bonding parameters for **2**

D	H	A	d(D-H)/Å	d(H-A)/Å	d(D-A)/Å	D-H-A/°
N2	H2	O2	0.851(14)	1.938(15)	2.7697(16)	165.6(19)
N4	H4	O3	0.841(15)	1.992(15)	2.8168(16)	167(2)
N6	H6	O1	0.869(15)	1.971(15)	2.8217(17)	165.8(19)

Table S6 Hydrogen bonding parameters for **3**

D	H	A	d(D-H)/Å	d(H-A)/Å	d(D-A)/Å	D-H-A/°
N2	H2	O2	0.867(15)	1.969(16)	2.820(2)	167(2)
N4	H4	O3	0.865(15)	1.917(16)	2.769(2)	168(2)
N6	H6	O1	0.853(15)	1.980(16)	2.815(2)	166(2)

Table S7 Hydrogen bonding parameters for **4**

D	H	A	d(D-H)/Å	d(H-A)/Å	d(D-A)/Å	D-H-A/°
N2	H2	Cl2	0.885(18)	2.50(2)	3.364(3)	166(4)
N4	H4	Cl2	0.860(19)	2.87(3)	3.541(4)	136(4)
N6	H6A	Cl1[1]	0.88	2.94	3.673(13)	141.9
N8	H8A	Cl1	0.88	2.87	3.609(18)	142.8
N8	H8A	Cl2[1]	0.88	3.05	3.67(2)	128.9

[1]1-*x*,1-*y*,1-*z*

Table S8 Hydrogen bonding parameters for **5**

D	H	A	d(D-H)/Å	d(H-A)/Å	d(D-A)/Å	D-H-A/°
O9	H9A	Cl6	0.87	2.27	3.089(5)	155.3
O9	H9B	Cl6[1]	0.87	2.26	3.090(5)	157.6
N4	H4	Cl1	0.88(2)	2.60(5)	3.306(6)	138(6)
N6	H6	Cl6[1]	0.90(2)	2.33(3)	3.194(8)	163(7)
N8	H8	Cl6	0.89(2)	2.58(5)	3.202(6)	128(5)
N10	H10	Cl6	0.88(2)	2.46(3)	3.322(6)	167(6)
N12	H12	Cl5	0.87(2)	2.30(3)	3.148(6)	165(6)
N14	H14A	Cl5	0.90(2)	2.23(3)	3.107(7)	164(6)
N16	H16A	Cl5	0.88(2)	2.33(4)	3.128(7)	152(6)

[1]1-*x*,1-*y*,-*z*;

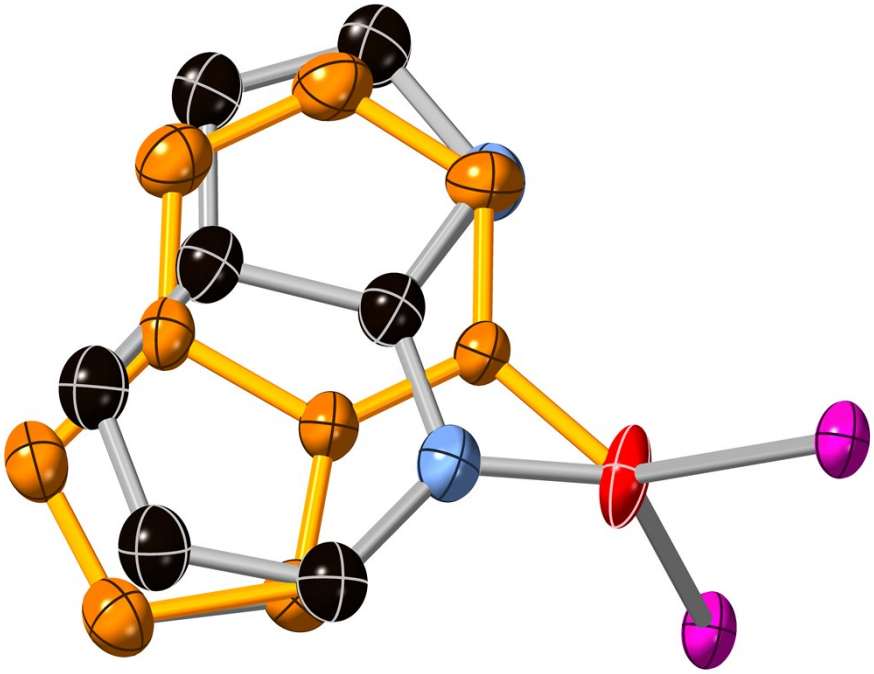

Figure S8 The disorder mode of the **HL** species in the structure of complex **4**. Hydrogen atoms are omitted for clarity and ADPs are rendered at 50% probability.

5. Additional Electronic Spectroscopy Figures and Data

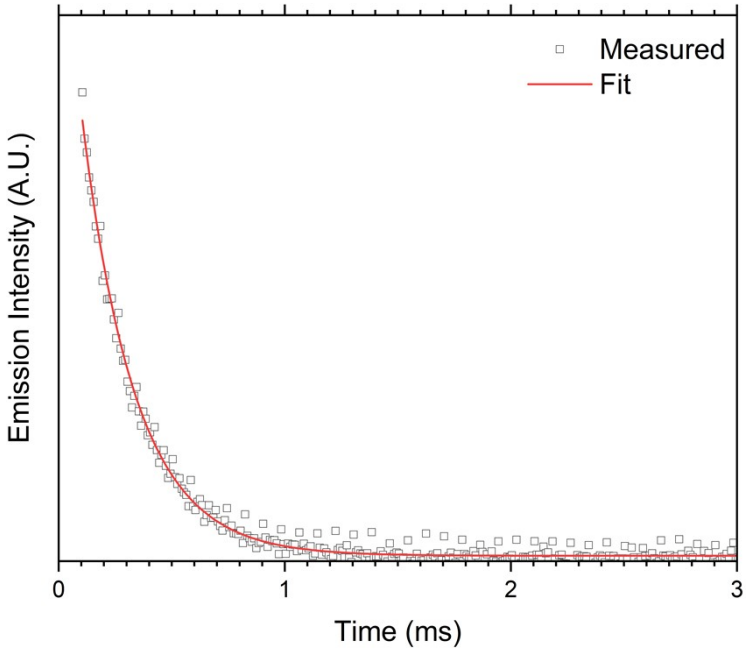

Figure S9 Measured phosphorescence decay curve (hollow squares) for the $^5D_0 \rightarrow {}^7F_2$ band (616 nm, λ_{ex} = 304 nm) in complex **2**. The measurement was taken at the conclusion of a titration experiment at an M:L ratio of 0.75:1 with an Eu^{3+} concentration of 24 μM. The red line represents the fit to the monoexponential function Intensity = $A_1e^{(-t/\tau 1)}$ + c, for A_1 = 9.969, c = 0.0784 and τ_1 = 0.235 ms

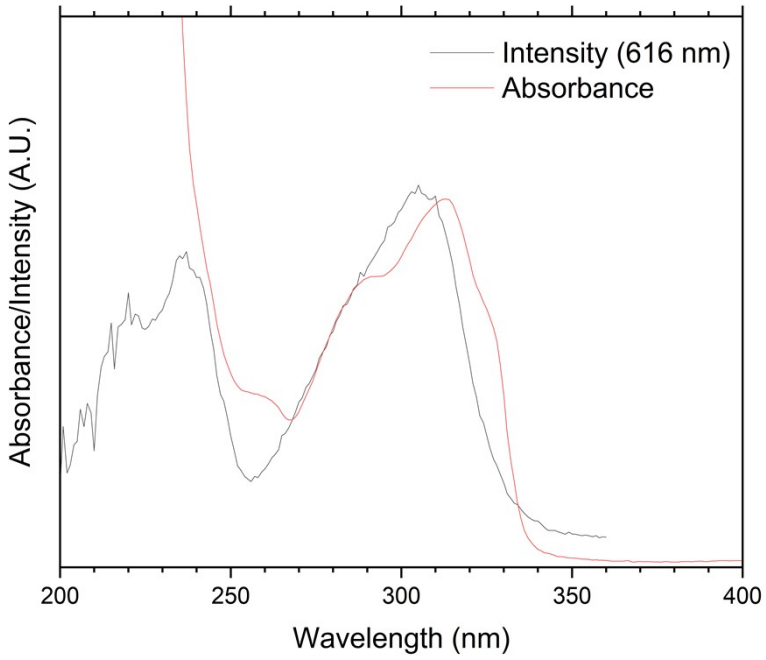

Figure S10 Overlaid absorption (red) and excitation (black, λ_{em} = 616 nm) spectra for complex **2** at the conclusion of a titration experiment at an M:L ratio 0.75:1 with an Eu^{3+} concentration of 24 μM. The absorbance profile in the range 350 – 250 nm is a combination of absorbance due to complex **2** and free **HL** in solution; at this concentration and M:L ratio, taking logβ_3 = 13.7 the ratio of **HL**:Eu(**HL**)$_3$ is approximately 3:1.

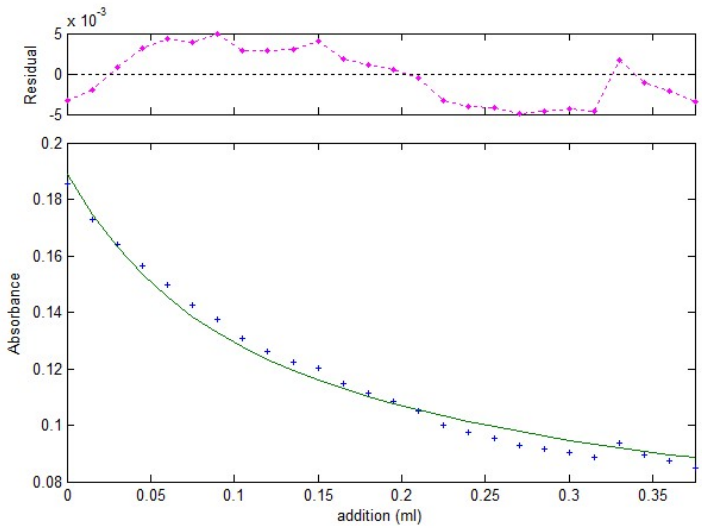

Figure S11 Representative binding isotherm (blue points, λ = 256nm) and fit (green line) from fitting the absorbance spectra for additions of europium nitrate aliquots to **HL** in acetonitrile (35 μM). The full x axis range corresponds to 0 – 0.7 equivalents of Eu^{3+} added, equivalent to a twofold excess for the formation of complex **2**.

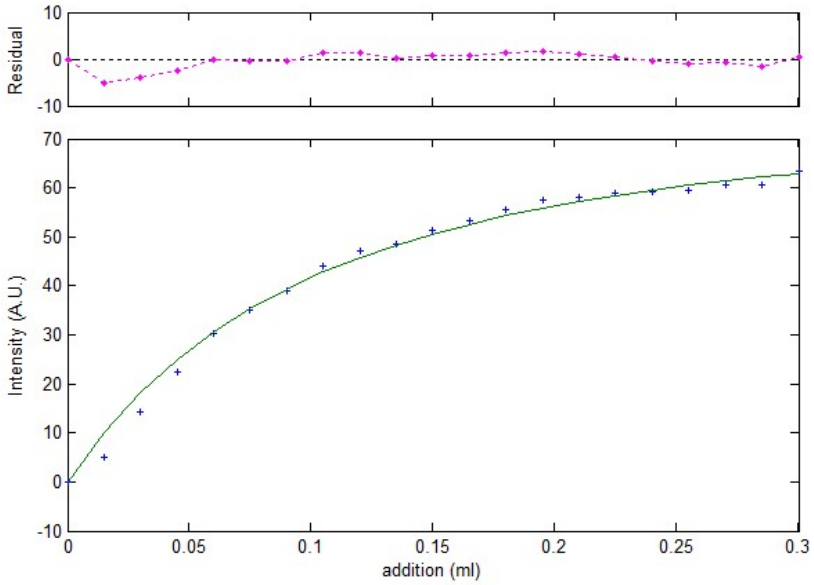

Figure S12 Representative binding isotherm (blue points) and fit (green line) from fitting the phosphorescence emission spectra (λ_{em} = 616 nm, λ_{ex} = 304 nm) for additions of europium nitrate aliquots to **HL** in acetonitrile (35 μM). The full x axis range corresponds to 0 – 0.75 equivalents of Eu^{3+} added, equivalent to a slightly above twofold excess for the formation of complex **2**.

6. Mass Spectrometry

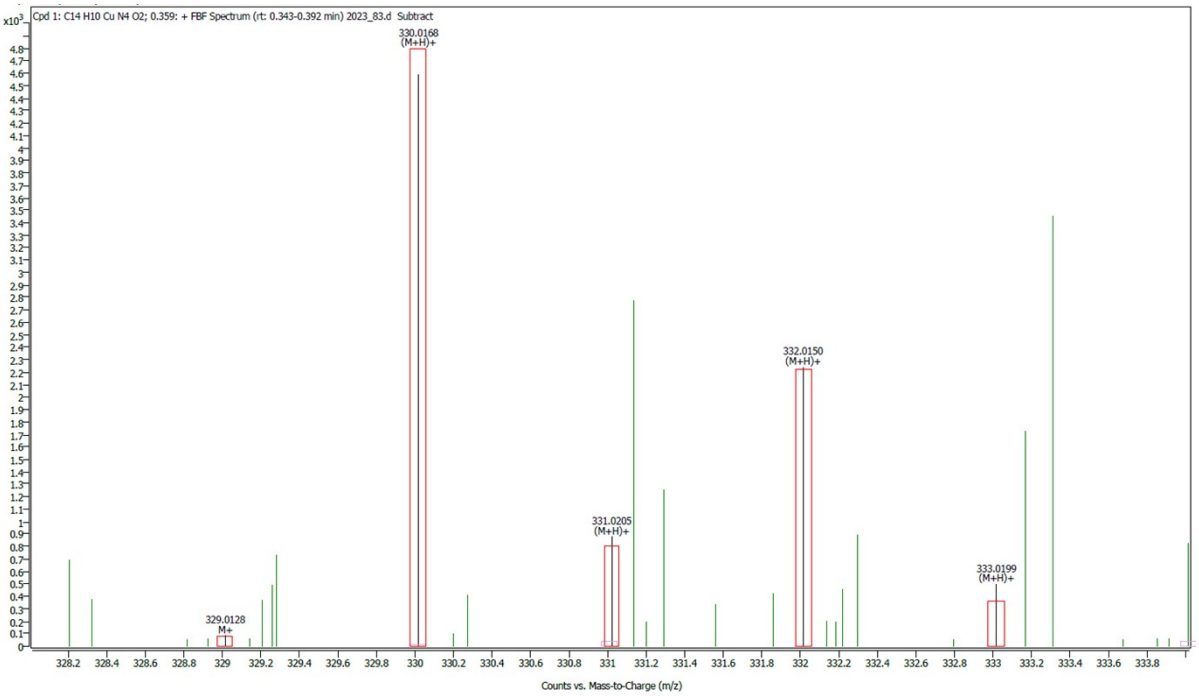

Figure S13 Isotopic distribution pattern observed by HRMS for complex **1** in methanol, with observed signal in black and coloured boxes representing simulated isotope pattern.

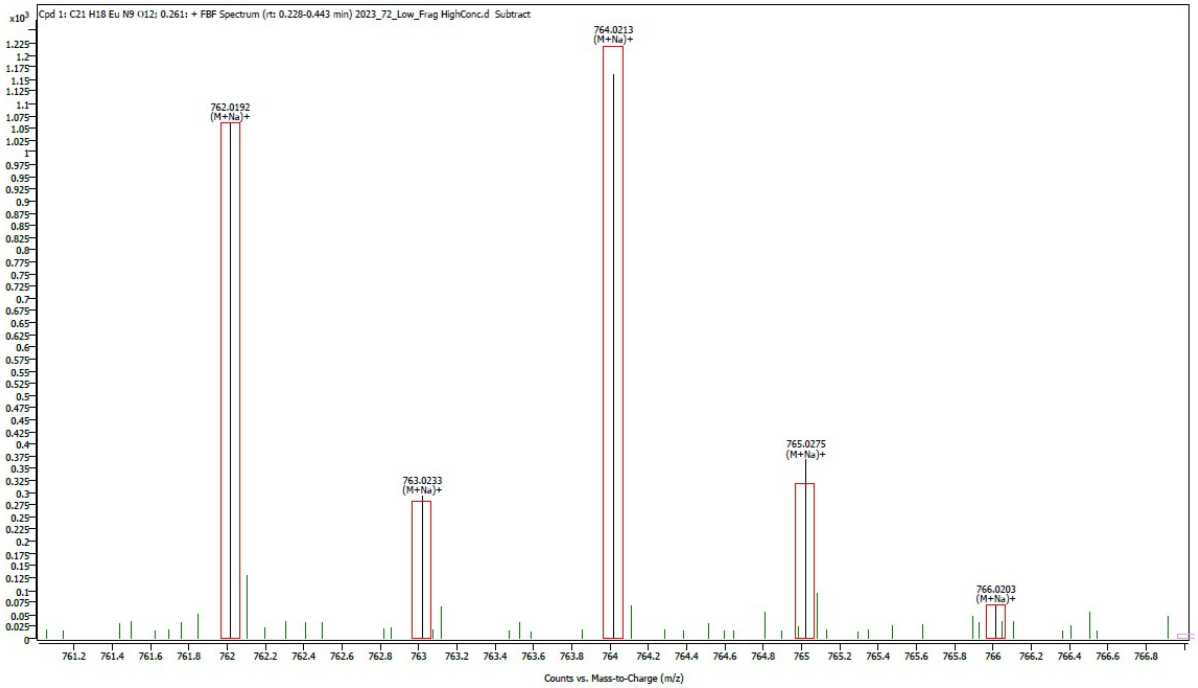

Figure S14 Isotopic distribution pattern observed by HRMS for complex **2** in acetonitrile, with observed signal in black and coloured boxes representing simulated isotope pattern.

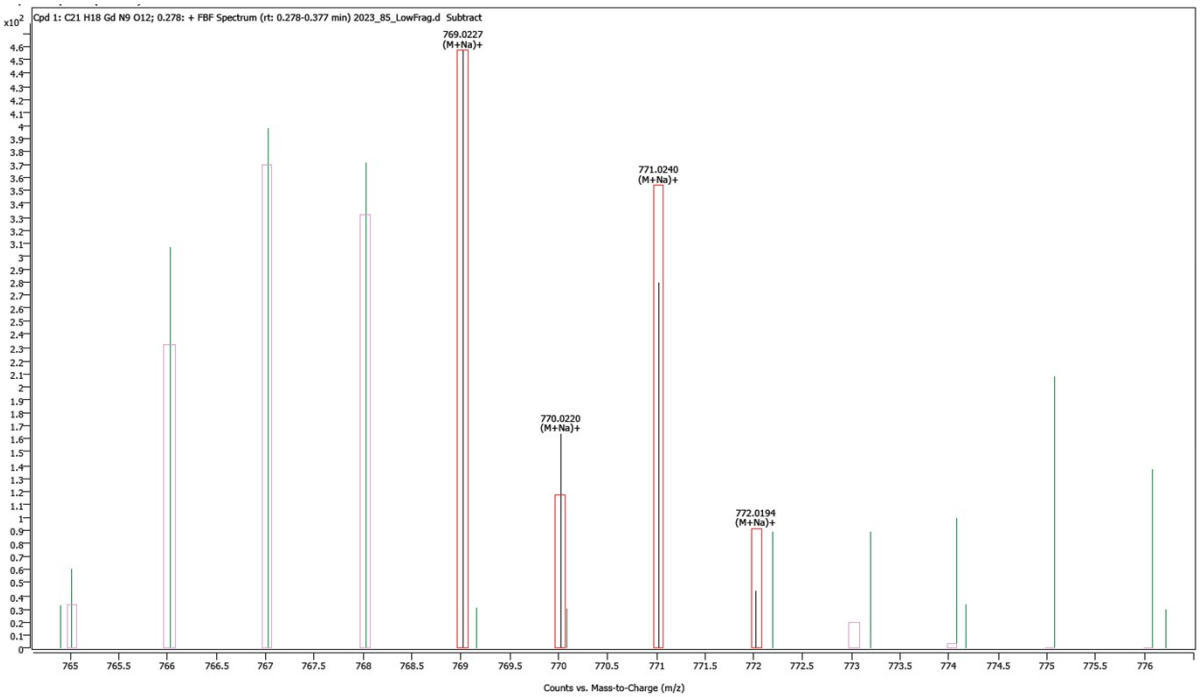

Figure S15 Isotopic distribution pattern observed by HRMS for complex **3** in acetonitrile, with observed signal in black and coloured boxes representing simulated isotope pattern.

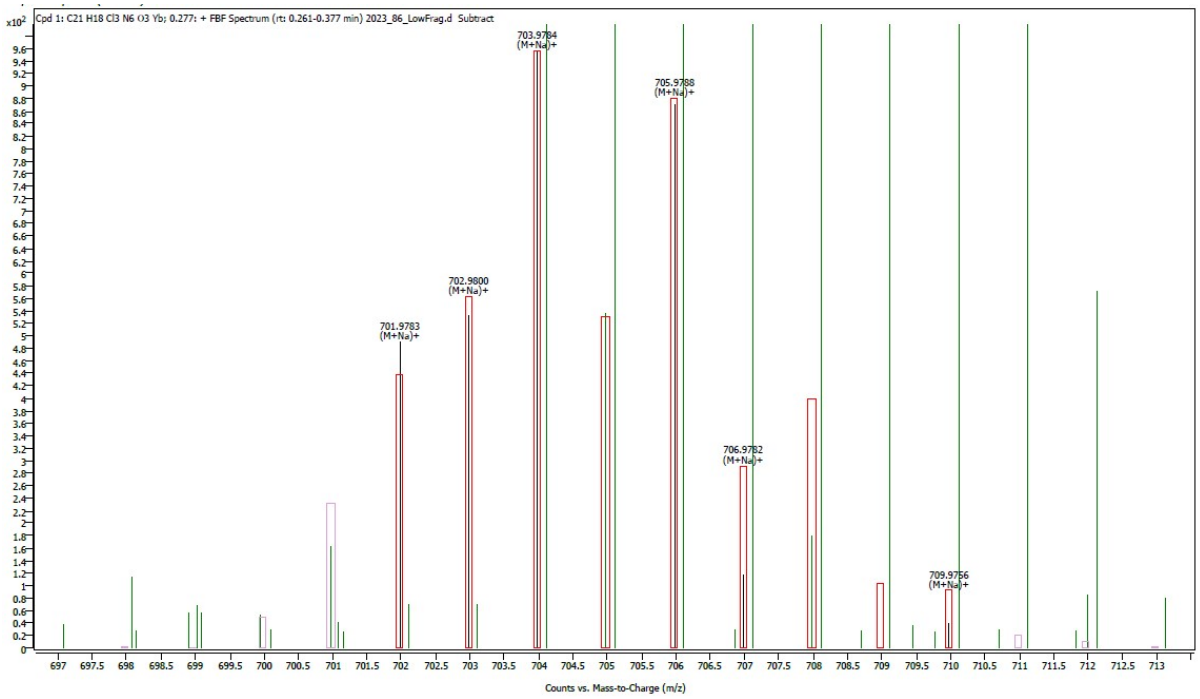

Figure S16 Isotopic distribution pattern observed by HRMS for complex **4** in acetonitrile, with observed signal in black and coloured boxes representing simulated isotope pattern.

7. References

S1. *ReactLab Equilibria,* Jplus Consulting Ltd, Fremantle, Australia, 2018.

S2. *Bruker APEX-3*, Bruker-AXS Inc., Madison, WI, 2016.

S3. SADABS 2016/2, Bruker-AXS Inc., Madison, WI, 2016.

S4. G. M. Sheldrick, *Acta Crystallogr., Sect. A: Found. Adv.,* 2015, **71**, 3–8.

S5. G. M. Sheldrick, *Acta Crystallogr., Sect. C: Struct. Chem.*, 2015, **71**, 3–8.

S6. O. V. Dolomanov, L. J. Bourhis, R. J. Gildea, J. A. K. Howard and H. Puschmann, *J. Appl. Crystallogr.*, 2009, **42**, 339–341.